ELSEVIER

Journal of Pharmaceutical and Biomedical Analysis
16 (1998) 741–751

JOURNAL OF
PHARMACEUTICAL
AND BIOMEDICAL
ANALYSIS

Structural elucidation and conformational properties of the immunomodulator linomide

Thomas Mavromoustakos [a,*], Maria Zervou [a], Dimitris Panagiotopoulos [a], Efthimia Theodoropoulou [a], John Matsoukas [b], Dimitrios Karussis [c]

[a] *Institute of Organic and Pharmaceutical Chemistry, National Hellenic Research Foundation, Vas. Constantinou 48, Athens 11635, Greece*
[b] *Department of Chemistry, University of Patras, Patras 26500, Greece*
[c] *Departments of Neurology and Neuroimmunology Research Unit, Hadassah, University Hospital and Hebrew University–Hadassah Medical School, Jerusalem, Israel*

Received 13 January 1997; received in revised form 7 April 1997

Abstract

Linomide is a new synthetic immunomodulator which exerts prominent anti-autoimmune effects in various experimental models. Recently, it was tested in clinical trials to patients suffering from multiple sclerosis and showed to inhibit the activity of the disease. Therefore, due to its pharmacological importance, we attempted elucidate its structure using one-dimensional and two-dimensional nuclear magnetic resonance (NMR) techniques and study its conformational properties using a combination of two-dimensional NMR spectroscopy and molecular modeling. The conformational analysis of linomide was based on the measurement of interproton nuclear Overhauser enhancement (NOE) values obtained from a two-dimensional NMR spectrum and a number of molecular modeling techniques used to calculate the low energy conformers of this compound. This information will serve as an aid to synthetic chemists whom their research activity is focused on developing linomide analogs with better biological profiles. © 1998 Elsevier Science B.V.

Keywords: High-resolution nuclear magnetic resonance (NMR) spectroscopy; Linomide; Molecular graphics; Quinoline-3-carboxamide

1. Introduction

Conventional therapy of multiple sclerosis and other autoimmune diseases is based on immunosuppressive agents. However, these agents usually induce several, long-term side-effects. Additionally, upon their discontinuation, the clinical symptoms often relapse [1–4]. Recently, alternative approaches to the treatment of autoimmunity utilizing modulators of the immune system are developed based on theories advocating the importance of immune networks for the preservation of an intact 'self' [5].

Linomide (Pharmacia, Sweden, Roquinimex/LS-2616) (Fig. 1) is a potent synthetic im-

* Corresponding author: Tel.: + 30 1 7253821; fax: + 30 1 7247913/7253821.

PII S0731-7085(97)00107-6

munomodulator compound (quinoline-3-carbox amide) that may represent an attractive agent for the treatment of autoimmune diseases. It stimulates several immune functions, including activation of non-MHC-restricted cytotoxicity (NK activity), increased ConA proliferation of lymphocytes and enhanced IL-2 production [6–9]. LS-2616 also exhibits antiviral properties, resulting in prevention of both direct mortality and secondary development of autoimmune myocarditis following coxsackie virus infection [10]. This synthetic analog prevents the metastatic disease in animal models of cancer, and promotes the amelioration of the autoimmune manifestations of lupus-like syndrome (in MRL/lpr and (NZBXNZW F1) and of collagen-induced arthritis in DBA mice [11–14].

In our previous studies, we tested the efficacy of linomide in modulating autoimmunity. This synthetic analog was tested using experimental autoimmune encephalomyelitis (EAE) as a prototype model for induced autoimmunity and other models, such as experimental autoimmune myasthenia gravis and type I autoimmune diabetes. The most important results from these studies are summarized below: (i) linomide can be administered orally, and is very well absorbed and tolerated; (ii) it is effective in chronic EAE and autoimmune diabetes even when given at advanced stages, after the appearance of the first clinical signs; (iii) it totally prevents histological damage to the target organ; and (iv) it is not associated with the long-term side-effects of conventional immunosuppressive agents [15–18]. In a recently completed clinical trial from the same department, it was shown that linomide inhibits the progression of disability and reduces the active lesions in the brain in patients with multiple sclerosis [19].

In the present study, we sought to elucidate the structure of linomide and study its conformational properties using a combination of nuclear magnetic resonance (NMR) spectroscopy and molecular modeling conformational search methods.

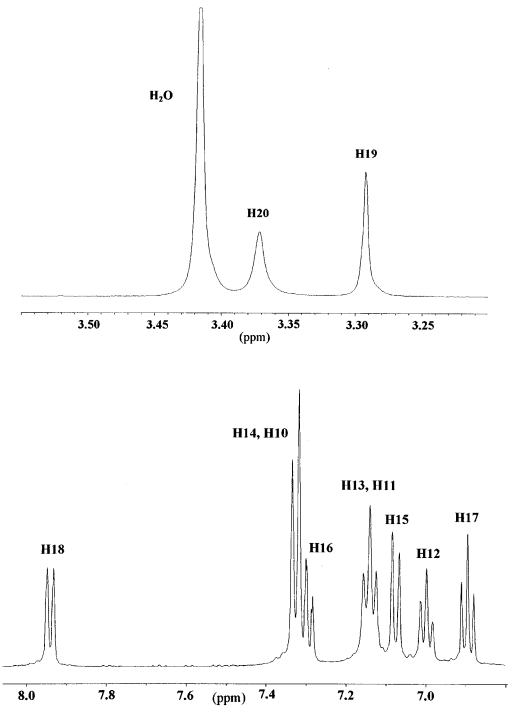

Fig. 2. ^{1}H-NMR spectrum of linomide in DMSO at 298 K recorded on a Bruker AC 300 MHz and DRX 500 MHz (aromatic region).

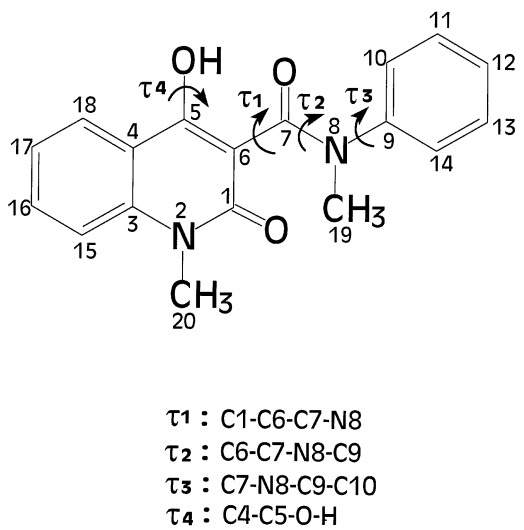

Fig. 1. Molecular structure of quinoline-3-carboxamide (linomide).

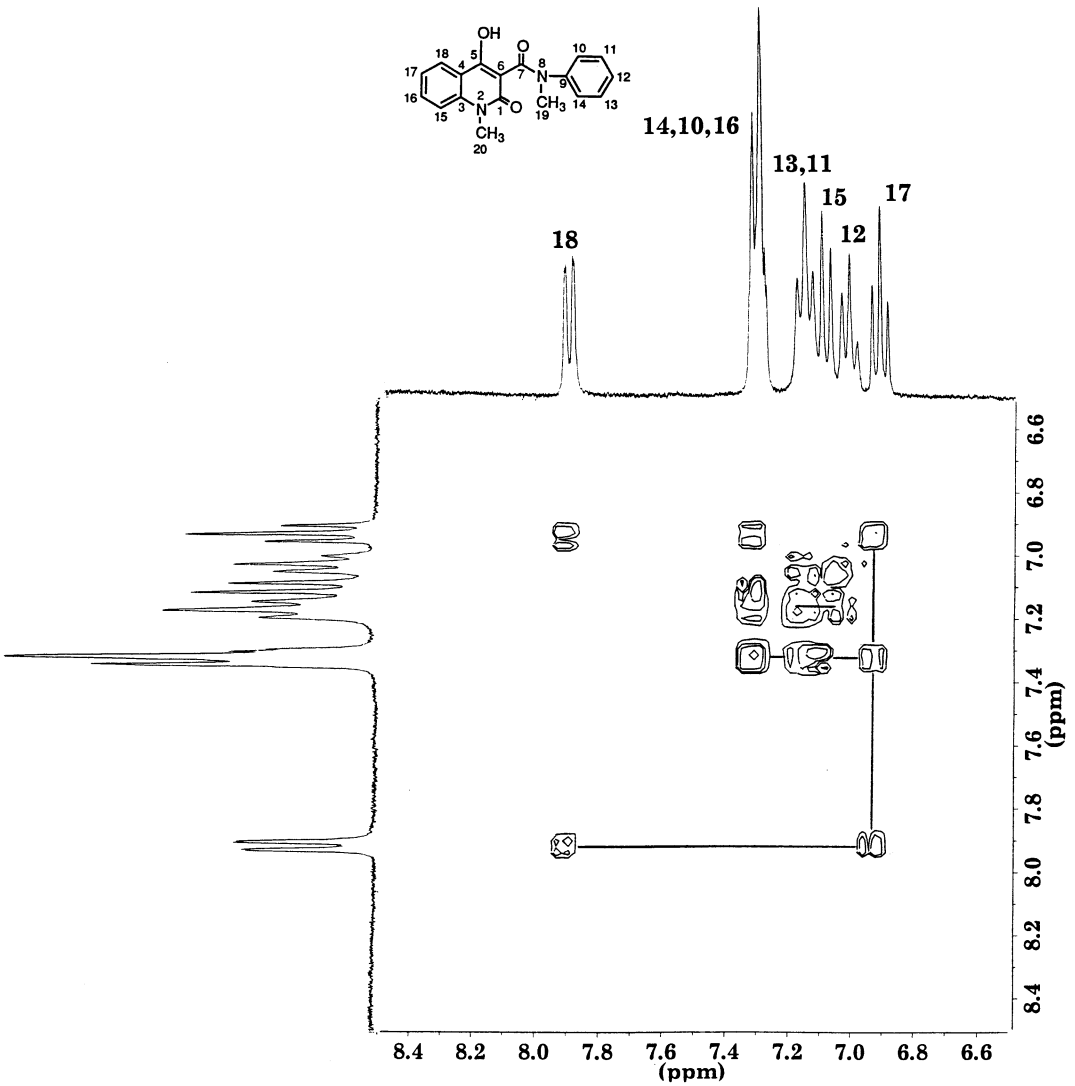

Fig. 3. COSY 45° spectrum of linomide in DMSO at 298 K recorded on a Bruker AC 300 MHz. The circled cross-peaks indicate the aromatic vicinal $^{1}H-^{1}H$ through bond interproton couplings.

2. Materials and methods

2.1. Materials

DMSO (99%+) and ultra-precision NMR tubes were purchased from SDS (Solvents Documentation Synthesis), Peypin, France.

2.2. NMR spectroscopy

The high-resolution spectra were obtained using Bruker 300 AC and 500 MHz DRX instruments. All data were collected using pulse sequences and phase-cycling routines provided in the Bruker library of pulse programs. Data processing, in-

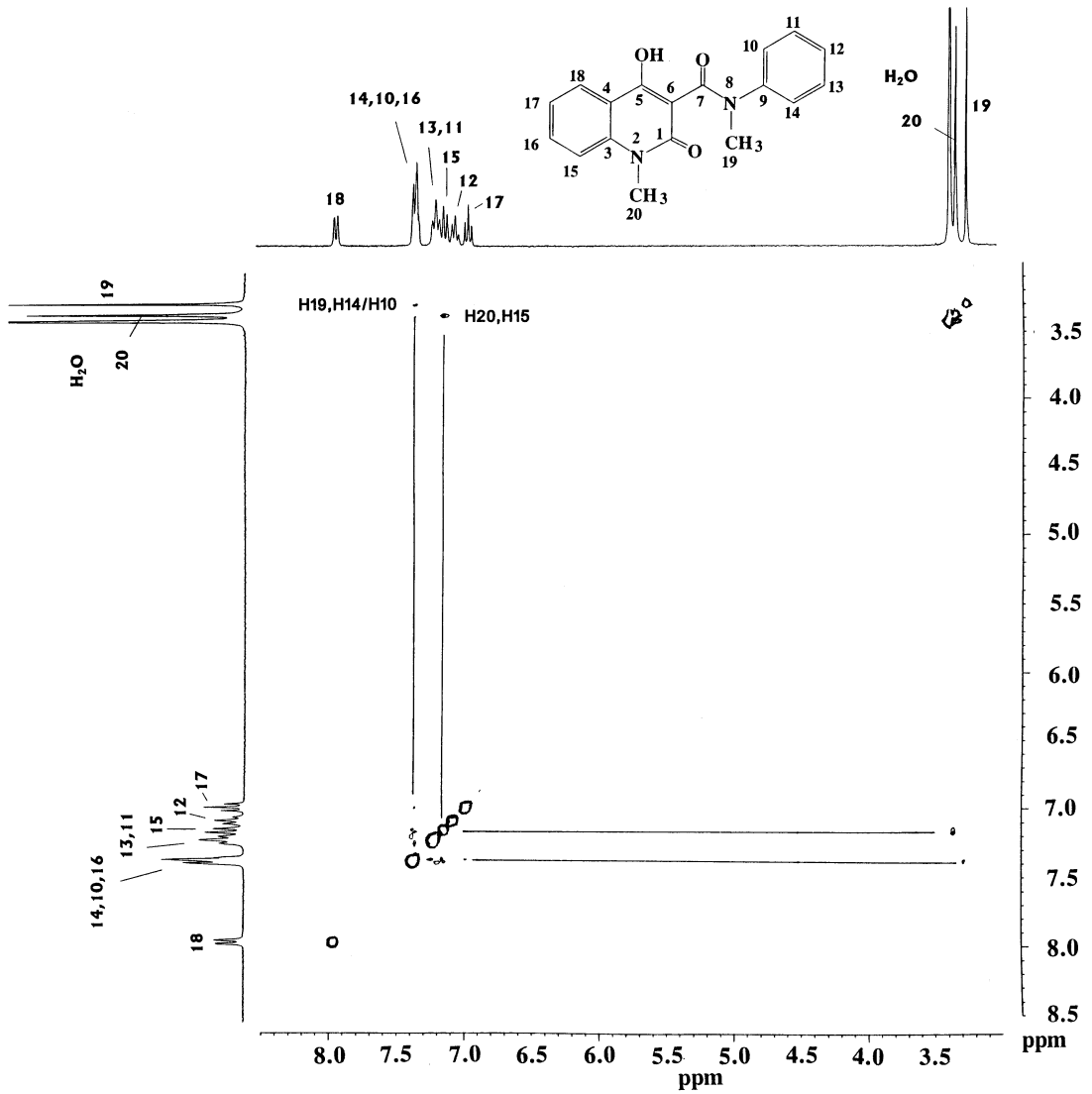

Fig. 4. NOESY spectrum of linomide in DMSO at 298 K recorded on a Bruker AC 300 MHz. The lines indicate the most useful $^{1}H-^{1}H$ through space interproton couplings.

cluding sine-bell apodization, Fourier transformation, symmetrization and plotting, were performed using Bruker software packages. ^{1}H-NMR spectra were recorded using the following acquisition parameters: pulse width (PW) 6.0 μs, spectral width (SW) 6024 Hz, data size (TD) 16K, recycling delay (RD) 1.0 s, number of transients (NS) 16, and digital resolution 0.735 Hz per point (Hz pt^{-1}). ^{13}C-NMR spectra were performed with PW 8.4 μs, SW 131 579 Hz, TD 16K, RD 9.4 s, NS 512 and digital resolution 0.803 Hz pt^{-1}. The $^{1}H-^{1}H$ correlation spectroscopy (COSY) spectrum was recorded using the following acquisition parameters: recycling delay (D1) 1 s, D0 increment 3 μs, spectral width in F_2 3571.43 Hz and in F_1 1785.71 Hz. The data sizes were 1K and 2K in

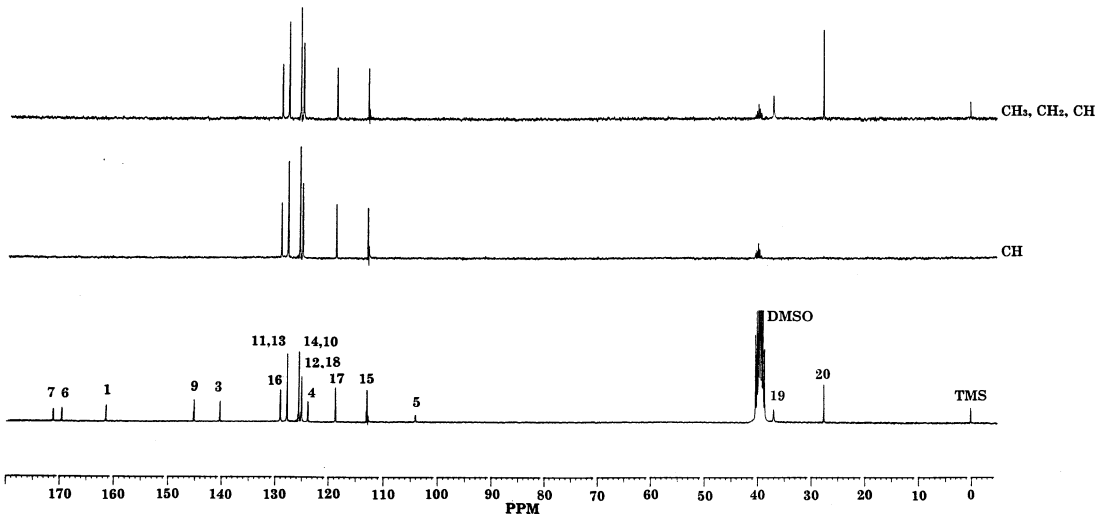

Fig. 5. ^{13}C-DEPT experiment of linomide in DMSO at 298 K recorded on a Bruker AC 300 MHz.

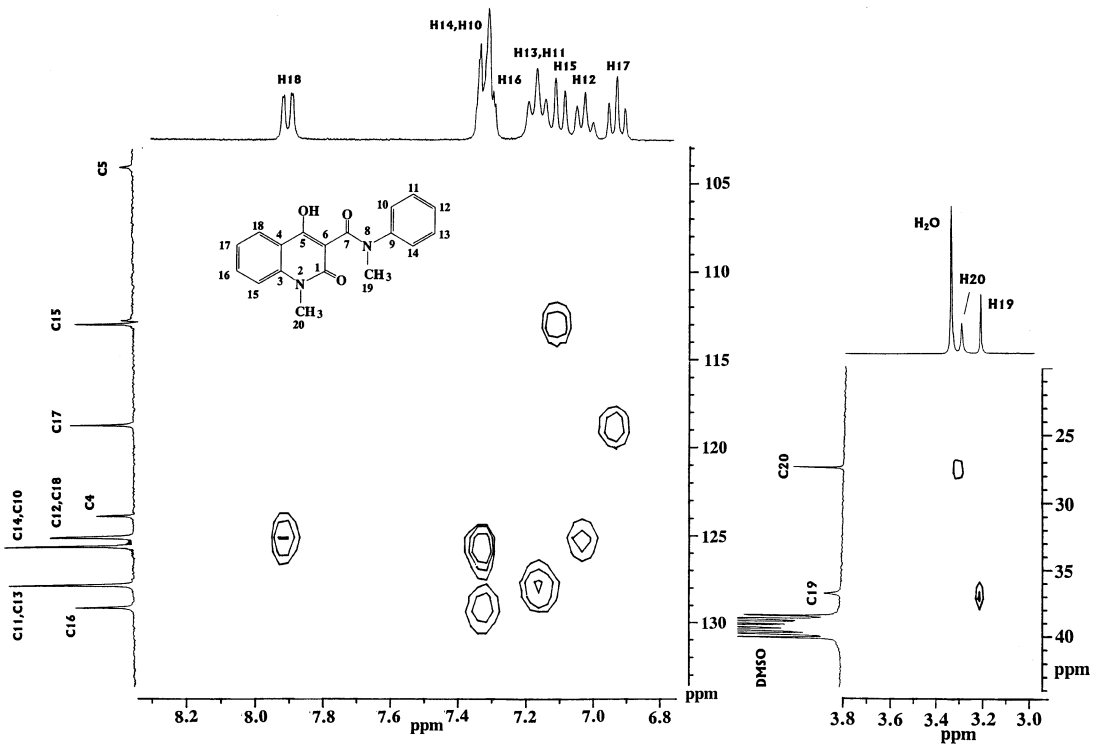

Fig. 6. Expanded regions of ^{13}C–^{1}H inverse correlation 2D experiment of linomide in DMSO at 298 recorded on a Bruker AC 300 MHz.

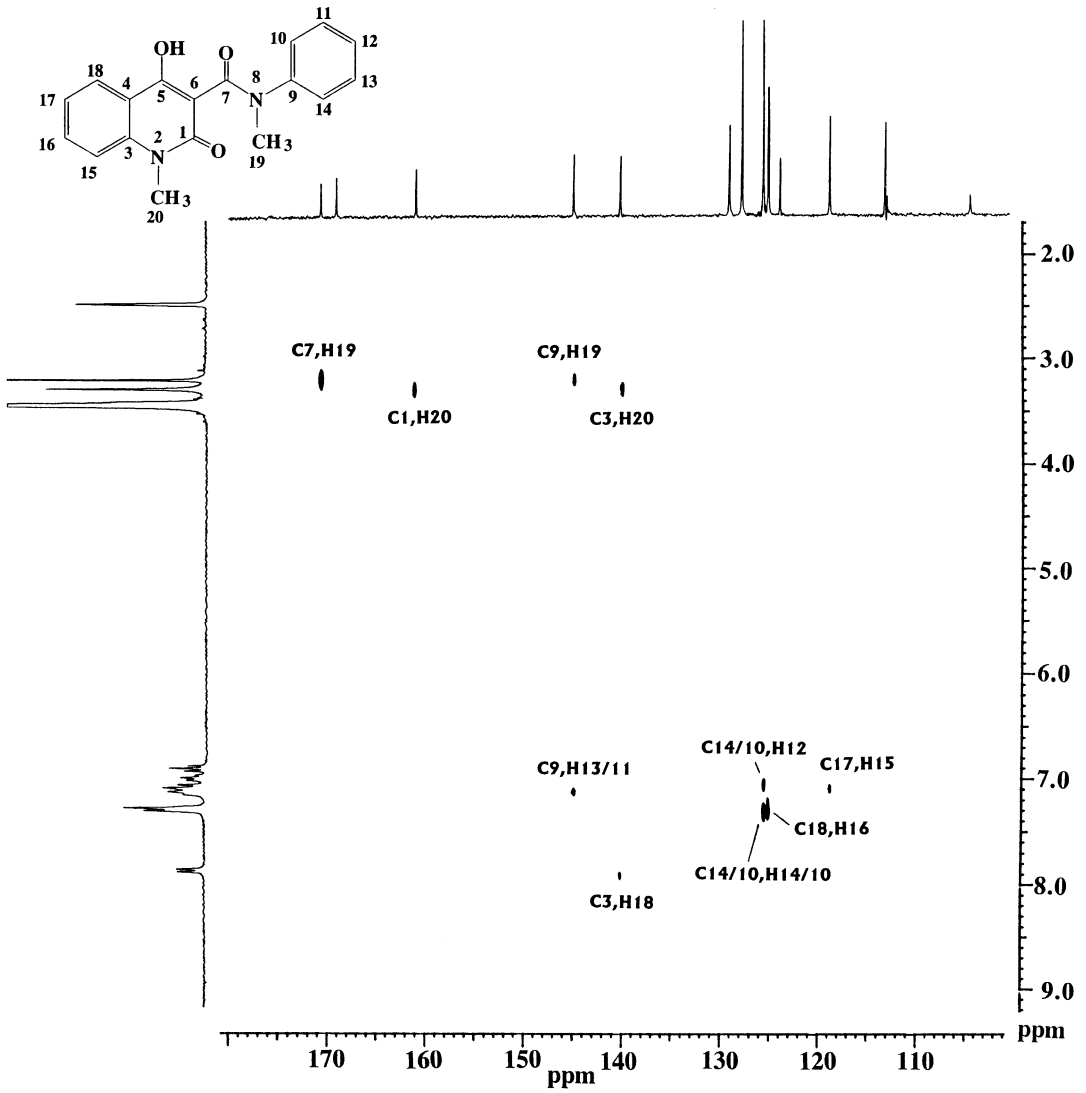

Fig. 7. A 2D $^{13}C-^{1}H$ COLOC experiment of linomide in DMSO at 298 K recorded on a Bruker AC 300 MHz.

F_1 and F_2, respectively, and the data were zero-filled in F_1 prior to 2D Fourier transformation to yield a $2 \times 2K$ data matrix. The spectrum was processed using a sine-bell window function both in F_1 and F_2 (WDW = S) and the data were symmetrized about the diagonal (SYM). Two-dimensional (2D) phase-sensitive $^{1}H-^{1}H$ nuclear Overhauser enhancement (NOESYPH) spectra were recorded using the following acquisition parameters: D1 = 1.0 s, D0 = 3 μs, SW in F_2 2551 Hz and F_1 1275.5 Hz. Several mixing times (0.1–1.0 s) were used in the NOESYPH experiment, of which 1.0 s gave the most prominent NOE results. Digital resolution was 2.0 Hz pt^{-1} in both directions. A $^{13}C-^{1}H$ inverse experiment was run using a bilinear rotation decoupling (BIRD) pulse sequence and the following acquisition parameters: D1 = 1.0 s, D0 = 3 μs, SW in F_2 3937 Hz and F_1 8223.7 Hz. The $1/2J$ $^{13}C-^{1}H$ time used was 35 ms. The data sizes were 256W and 1K in F_1 and F_2,

Table 1
Dihedral descriptors of the 11 lowest energy conformers derived from molecular dynamics

Conformers	τ_1	τ_2	τ_3	τ_4
A	−84.7	−178.6	69.9	128.6
B	−93.9	−173.7	66.4	−152.1
C	−77.1	174.7	74.2	107.8
D	−111.1	−163.7	79.4	−109.8
E	−90.6	−170.9	62.7	−137.7
F	−106.8	−164.2	66.8	−110.8
G	−75.6	171.3	80.0	99.2
H	−73.7	166.0	86.7	97.5
K	−74.1	163.9	88.5	94.9
L	−72.3	156.8	116.6	−123.4
M	−76.6	157.5	110.1	101.1

respectively, and the data were zero-filled in F_1 prior to 2D Fourier transformation to yield a 2K × 512W data matrix. The Hz pt^{-1} in F_2 dimension/Hz pt^{-1} in F_1 dimension (I2D) was 0.120. $^{13}C-^{1}H$ shift correlation by long-range coupling (COLOC) was used with the following acquisition parameters: D1 = 2.0 s, D0 = 3 μs, SW in F_2 1497 Hz and F_1 20 000 Hz. The $1/2J$ $^{13}C-^{1}H$ time used was 0.05 s (D2). The data sizes were 256W in F_1 and 4K in F_2.

2.3. Molecular modeling

Computer calculations were performed on a Silicon Graphics 4D/35 using the QUANTA 3.3 version of the Molecular Simulation Incorporated (MSI) program. The conformational energy of linomide was first minimized and then subjected to conformational search methods to explore its lower energy conformers. Thus, a conformational grid search method was applied to each of the critical dihedral angles ($\tau_1-\tau_4$) coupled with molecular dynamics. The dynamics experiment was run using a dielectric constant that simulates the DMSO environment ($\varepsilon = 45$) and simulation time 2 ps at a temperature of 1000 K. Eleven family structures were generated using the dihedral angle criterion ($\approx 40°$) ($R_{max} = 112.7$, $R_{min} = 0.8$). The lowest energy conformers from each family were considered as representative conformers [20,21].

3. Results and discussion

3.1. Structural identification of linomide

Fig. 2 depicts the ^{1}H-NMR spectrum of lino-

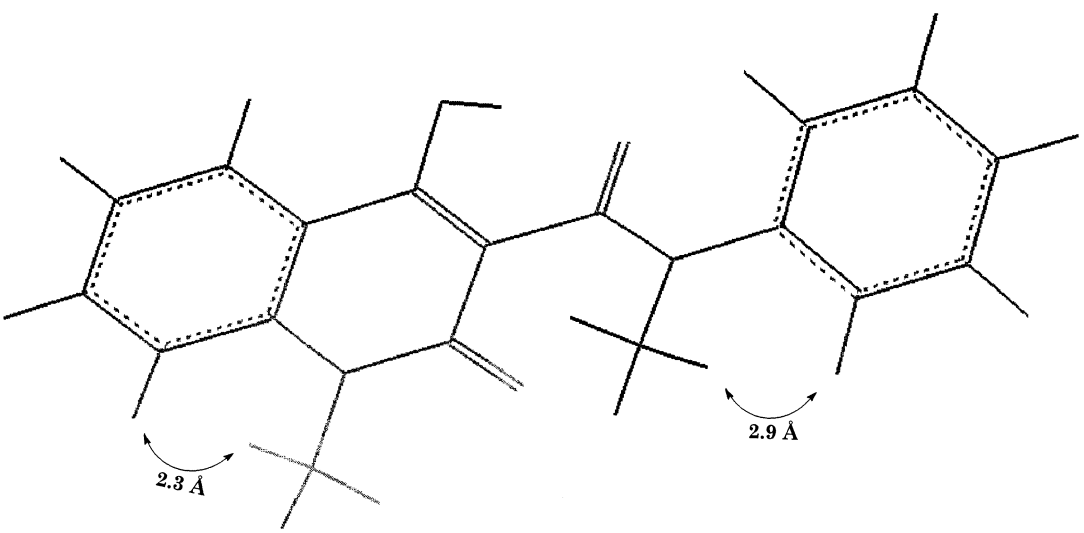

Fig. 8. Representative lowest energy conformer derived from 11 family structures obtained after performing dynamics at a simulated temperature of 1000 K.

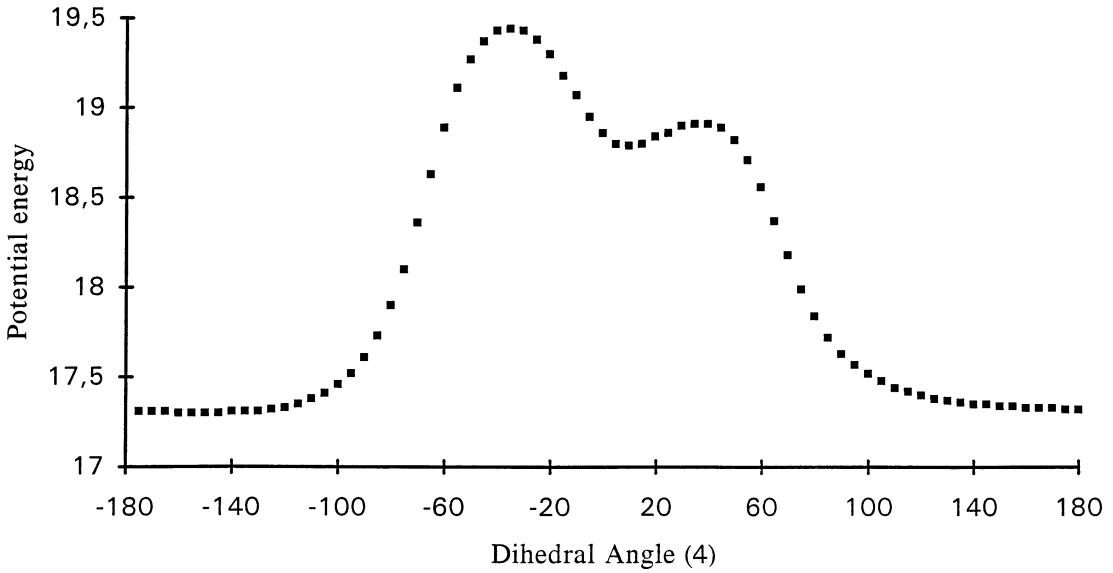

Fig. 9. Conformational energy profile (kcal mol^{-1}) as a function of C4–C5–O3–H (τ_4 dihedral angle) obtained from a grid search scan with increments of 5°.

mide in DMSO solvent. Observed peaks are referenced to tetramethylsilane (TMS). The assignment of the peaks is shown on the top of the spectrum. The peak identification was confirmed by integration of the peaks and a 2D COSY spectrum. The aromatic vicinal $^1H-^1H$ through bond interproton couplings of the 2D COSY experiment are shown with drawn lines in Fig. 3.

The proton structural assignments were also aided by a NOESY experiment. Thus, H19 and H20 protons were assigned unambiguously based on their NOE effects with H14 and H15, respectively. The critical NOEs are shown in Fig. 4. The combination of COSY and NOESY results establish structural assignments of all protons within the molecule.

The ^{13}C-NMR signals were assigned unambiguously on the basis of a distortionless enhancement by polarization transfer (DEPT), a 2D inverse $^{13}C-^1H$ correlation and long-range coupling COLOC experiments. DEPT experiment is useful as a pilot experiment to distinguish the different kind of carbons (Fig. 5). The inverse $^{13}C-^1H$ correlation experiment was run using the BIRD pulse sequence and aided to assign unambiguously the CH and CH_3 carbons. Expanded regions of this experiment are shown in Fig. 6. The COLOC experiment (Fig. 7) aided the unambiguous assignment of C1, C3, C7 and C9 carbons. Thus, C7 was differentiated from C1 based on the long couplings C7–H19 and C1–H20. C9 was differentiated from C3 based on the long couplings C9–H19, C9–H13/H11, C3–H20 and C3–H18. Other long-range couplings observed in the COLOC experiment confirmed our structural assignments derived from the inverse $^{13}C-^1H$ correlation experiment.

3.2. Conformational properties of linomide

The observed NOEs H19–H14 and H15–H20 are critical for the conformational analysis of this molecule because they establish spatial vicinity between *N*-methyl hydrogens and those of the phenyl rings.

The NMR results were coupled with theoretical calculations. The energy of linomide was first minimized using the algorithm of steepest descents (SD) to approach its local minimum and

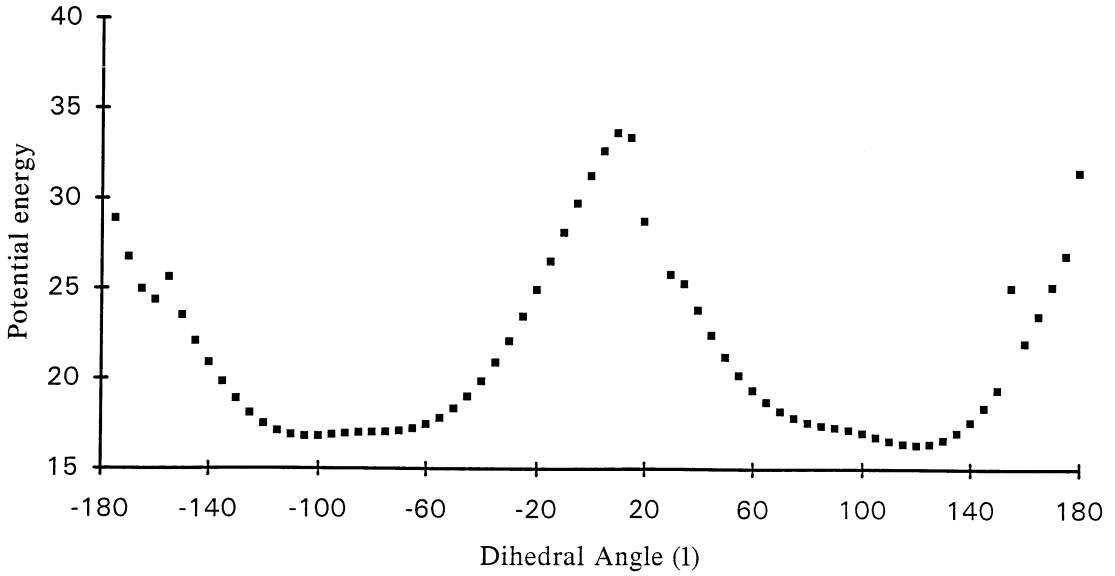

Fig. 10. Conformational energy profile (kcal mol^{-1}) as a function of C1–C6–C7–N8 (τ_1 dihedral angle) obtained from a grid search scan with increments of 5°.

then using the Newton Raphson (NR) method to reach the local minimum. The minimized structure was used in the dynamics experiment. The values of the dihedral angles of the lowest energy conformers derived from 11 family structures are shown in Table 1.

The two carbonyls in these conformers are almost perpendicular to each other, as is shown from the lowest energy values adopted by the τ_1 dihedral angle. This spatial relation between the two carbonyls minimizes their electrostatic repulsions. The combination of τ_1, τ_2 and τ_3 dihedral angles brings the *N*-methyl group almost in a perpendicular position to the phenyl ring. This avoids any electrostatic repulsions between the methyl group and the phenyl ring. The 11 lowest energy structures obtained differ by 1–3 kcal mol^{-1}. Only few low-energy conformers show a possibility of 'intermolecular' hydrogen bonding between the vinyl hydroxyl group and the carboxyl group. In the 11 conformers obtained, the distances between H14–H19 and H15–H20 were calculated. These were found to be in the ranges 2–3 and 3–4 Å. Thus, all 11 lowest energy conformers explain the observed experimental NOEs. Fig. 8 shows the lowest energy conformer with the calculated distances between H14–H19 and H15–H20 protons.

An exhaustive conformational grid search method was used to obtain the conformational energy profile (kcal mol^{-1}) of its critical torsion angles τ_1, τ_2, τ_3 and τ_4. This would provide detailed information about the conformational barriers that exist in the molecule.

The potential energy profile as a function of C4–C5–O–H (τ_4 dihedral angle) is shown in Fig. 9. The minimal values of τ_4 range between 100–180° and (−)100–(−)180°. However, the energy barrier between minimum and maximum values is only 2 kcal mol^{-1}. Thus, it appears that τ_4 has a high flexibility and can assume virtually any theoretical value. The possible potential energy values of C1–C6–C7–N8 (τ_1 dihedral angle) are depicted in Fig. 10. The barrier between the minimum and maximum values ranges about 18 kcal mol^{-1}. Therefore, this torsion angle adopts preferred values between (−)140–(−)60° and 60–140°. The obtained potential energy values for

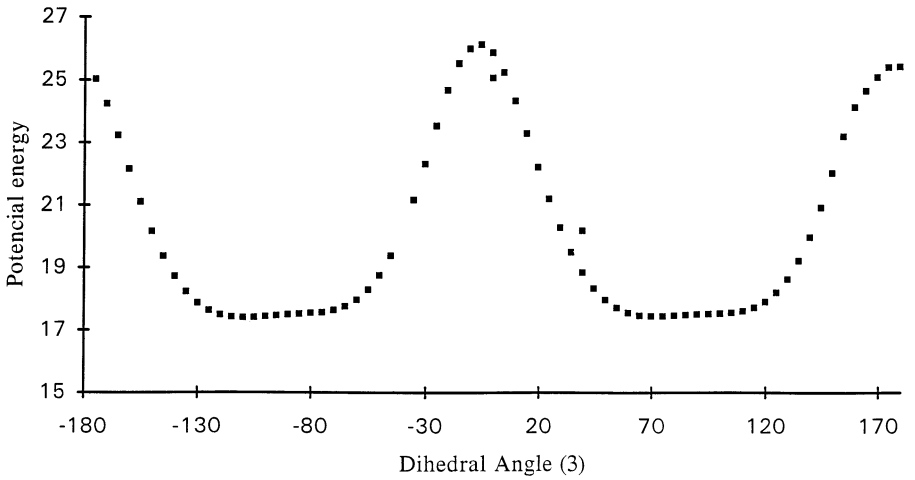

Fig. 11. Conformational energy profile (kcal mol^{-1}) as a function of C6–C7–N8–C9 (τ_2 dihedral angle) obtained from a grid search scan with increments of 5°.

C7–N8–C9–C10 (τ_3 dihedral angle) shown in Fig. 11 resemble those obtained in the energy profile as a function of τ_1. The high barrier between the minimum and maximum energy values reflects the high preference of the molecule to adopt limited low-energy values, (−)60–(−)100° and 100–140°. The potential energy as a function of C6–C7–N8–C9 (τ_2 dihedral angle) is shown in Fig. 12. The potential energy range in this profile is about 13 kcal mol^{-1}. The lowest energy values appear between 160 and 180°. Several other values appear as local minima.

A comparison between the potential energy profiles of individual critical dihedral angles in

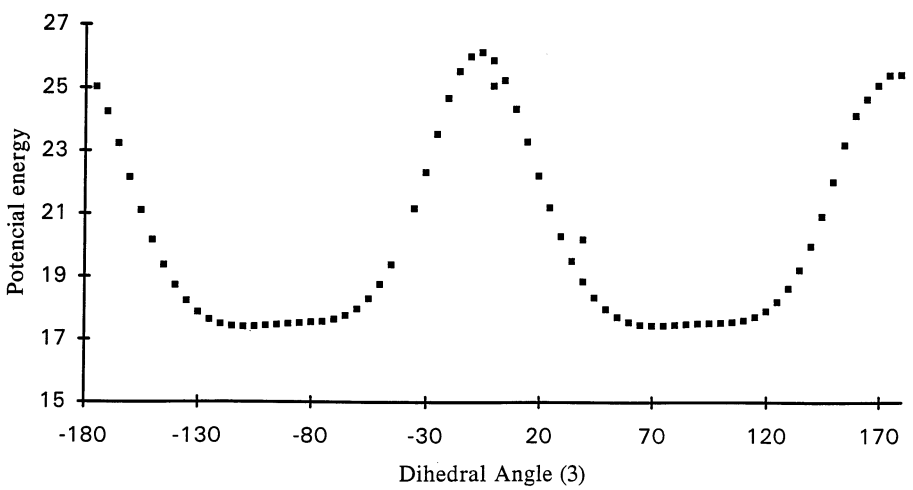

Fig. 12. Conformational energy profile (kcal mol^{-1}) as a function of C7–N8–C9–C10 (τ_3 dihedral angle) obtained from a grid search scan with increments of 5°.

Table 1 shows that the 11 lowest energy conformers contain combinations ffiof dihedral angles that fall in the lowest energy range of the potential energy profiles.

4. Conclusions

The conformational analysis of linomide in DMSO solvent showed that this molecule adopts low-energy conformers in which the two carbonyl groups minimize their electrostatic repulsions. The *N*-methyl attached to the phenyl ring is situated between the two carbonyls and the phenyl ring is in a position that also minimizes its electrostatic repulsions. The torsion angles τ_1, τ_2 and τ_3 adopt only a limited number of values that correspond to low-energy conformers. This conclusion is also confirmed by a dynamics experiment. The phenyl ring attached to carboxamide appears with only some flexibility. The angle τ_4 has no limit in its value since its maximum energy differs only by 2 kcal mol^{-1} when compared to its minimum one. This energy difference can be easily overcome in a biological environment. A hydrogen bonding between the vinyl hydroxyl group and the carbonyl group is not favored according to the observed low-energy conformers derived in the dynamics experiment and using an environment that simulates that of DMSO.

The information obtained regarding the conformational properties of linomide may be of aid to synthetic chemists who wish to develop linomide analogs with better biological profiles, as well as constrained analogs that adopt low-energy dihedral angles.

Acknowledgements

This work is supported mainly by the National Hellenic Research Foundation and the European Community Grants BIOMED No. 920038, BIOMED-PECO No. 930158 and COPERNICUS No. 940238.

References

[1] P.Y. Peterson, G.D. Drobish, Science 165 (1969) 191–192.
[2] M. Staykova, I. Goranov, T. Nikolov, Ann. Immunol. 129 (1978) 415–427.
[3] G.B. Schuller-Levis, P.B. Kozlowsky, H.M. Wisniewski, Clin. Immunol. Immunopathol. 40 (1986) 244–252.
[4] C. Feurer, C. Chow, F. Borel, Immunology 63 (1988) 219–223.
[5] O. Lieder, T. Reshef, E. Beraund, A. Ben-Nun, T.R. Cohen, Science 239 (1988) 181–183.
[6] T. Stalhandske, E. Eriksson, G.M. Sandberg, Int. J. Immunopharmacol. 4 (1982) 336.
[7] T. Kalland, G. Alm, T. Stalhandske, J. Immunol. 134 (1985) 3956–3961.
[8] T. Kalland, J. Immunol. 144 (1990) 4472–4476.
[9] T. Kalland, Cancer Res. 46 (1986) 3018–3022.
[10] N.G. Ilbaeck, J. Fohlman, S. Slorah, G. Friman, J. Immunol. 142 (1989) 3225–3228.
[11] S. Strober, K. Botzin, E. Field et al., Ann. N.Y. Acad. Sci. 475 (1986) 285-295.
[12] A. Tarkowski, K. Gunnarsson, L.A. Nilsson, L. Lindholm, T. Stalhandske, Arthritis Rheum. 29 (1986) 1405–1409.
[13] A. Tarkowski, K. Gunnarsson, T. Stalhandske, Immunology 59 (1986) 589–594.
[14] D.M. Karussis, D. Lehman, S. Slavin, U. Vourka-Karussis, R. Mizrachi-Koll, H. Ovadia, A. Ben-Nun, T. Kalland, O. Abramsky, Ann. Neurol. 34 (1993) 654–660.
[15] D.M. Karussis, D. Lehman, S. Slavin, U. Vourka-Karussis, R. Mizrachi-Koll, H. Ovadia, T. Kalland, O. Abramsky, Proc. Natl. Acad. Sci. 90 (14) (1993) 6400–6404.
[16] D.M. Karussis, Y. Lehman, R. Wirguin, R. Mizrachi-Koll, O. Abramsky, T. Brenner, J. Neuroimmunol. 55 (1994) 187–193.
[17] D.M. Karussis, D. Lehman, A. Linde, P. Gjostrup, O. Abramsky, Neurology 46 (Suppl. S) (1996) A252.
[18] D.M. Karussis, Z. Meiner, D. Lehman, J.M. Gomori, A. Schwarz, A. Linde, P. Gjorstrup, O. Abramsky, Neurology 45 (1995) 417–421.
[19] D.M. Karussis, Z. Meiner, D. Lehman, J.M. Gomori, A. Schwarz, A. Linde, O. Abramsky, Neurology 47 (1996) 341–346.
[20] J. Matsoukas, J. Hondrelis, M. Keramida, R. Yamdagri, Q. Wu, T. Mavromoustakos, A. Makriyannis, G. Moore, J. Biol. Chem. 269 (1994) 5303–5312.
[21] T. Mavromoustakos, D.-P. Yang, E. Theodoropoulou, A. Makriyannis, Eur. J. Med. Chem. 30 (1995) 227–234.